IEEE Access
Multidisciplinary | Rapid Review | Open Access Journal

Received March 12, 2018, accepted April 4, 2018, date of publication April 10, 2018, date of current version May 9, 2018.

Digital Object Identifier 10.1109/ACCESS.2018.2825256

ARMA-Based Adaptive Coding Transmission Over Millimeter-Wave Channel for Integrated Satellite-Terrestrial Networks

SHUSHI GU, JIAN JIAO, (Member, IEEE), ZIXUAN HUANG, SHAOHUA WU, (Member, IEEE), AND QINYU ZHANG, (Senior Member, IEEE)

Communication Engineering Research Center, Harbin Institute of Technology (Shenzhen), Guangdong 518055, China

Corresponding authors: Jian Jiao (jiaojian@hit.edu.cn) and Qinyu Zhang (zqy@hit.edu.cn)

This work was supported in part by the National Natural Sciences Foundation of China under Grant 61771158, Grant 61701136, Grant 61525103, and Grant 61371102, and in part by the Shenzhen Basic Research Program under Grant JCYJ20170811154309920, Grant JCY2017081114233370, Grant JCYJ20170811160142808, Grant ZDSYS20170728090330586, and Grant JCYJ20160328163327348.

ABSTRACT The integrated satellite-terrestrial network can provide broadband wireless access in a wide coverage, efficient, and cost-effective manner, and is regarded as one of the most promising infrastructures for future heterogeneous network toward fifth generation. With the development of next generation of high throughput satellites (HTS), the application of the millimeter-wave (mmWave) band HTS is viewed as a vital role in the future integrated satellite-terrestrial network. Considering the rain attenuation is the dominant fading factor of the mmWave channel, we first propose a practical time-varying rain attenuation prediction model based on the autoregressive-moving-average (ARMA) model. Then, we develop an adaptive coding transmission (ACT) scheme based on the analog fountain codes combine the ARMA mmWave channel prediction model. The key parameters are selected based on a tradeoff between the decoding failure probability, block length, and overhead for our ARMA-based ACT scheme. Simulation results show that our proposed ACT scheme can effectively improve the throughput.

INDEX TERMS Integrated satellite-terrestrial network, millimeter-wave channel, autoregressive-moving-average model, rain attenuation, adaptive coding transmission.

I. INTRODUCTION

Millimeter-wave (mmWave) band high throughput satellites (HTS) are viewed as backbone relays to enhance the throughput of the integrated satellite-terrestrial networks towards fifth generation (5G) [1], [2]. The architecture of future integrated satellite-terrestrial networks is shown in Fig. 1, where several mmWave band (e.g., Ka/Q/V-band) high-throughput geostationary Earth orbit (GEO) satellites can be connected to form the backbone network, and to support global ubiquitous broadband wireless access of the integrated space/air/terrestrial information network in the future [3], [4].

However, the mmWave band HTS return channel is known to be much more sensitive to the atmospheric attenuation than the conventional S/C/X-band channels [5], [6]. In order to further enhance the throughput of the mmWave channel, several optimization schemes have been proposed [7]–[9]. In particular, the rain attenuation at the Ka-band is much higher than at the X-band (in the order of 1.5 $\sim$ 4.5 dB/km higher for a rain rate ranging from 10 $\sim$ 30 mm/hour [10]). Thus, appropriate link margins should be allocated to take into account these atmospheric impairments and to reduce the target outage probability [11].

There are a number of advanced link designs that have been proposed in the literature to mitigate the effect of rain attenuation and system noise temperature on the Ka-band HTS return channel [12], [13]. Moreover, compared to the terrestrial communications, the space nodes in the integrated satellite-terrestrial networks are limited by resource limitations with respect to performing complicated rain attenuation prediction algorithms [14]. In general, a timely decision on the short-term weather state greatly complicates communication system operations [15].

Furthermore, space communications suffer from the long propagation delay, and conventional Automatic RepeatreQuest (ARQ) schemes are inefficient. In fact, the Consultative Committee for Space Data System (CCSDS) File Delivery Protocol (CFDP) and the Licklider Transport Protocol (LTP) are designed with a negative-acknowledgement

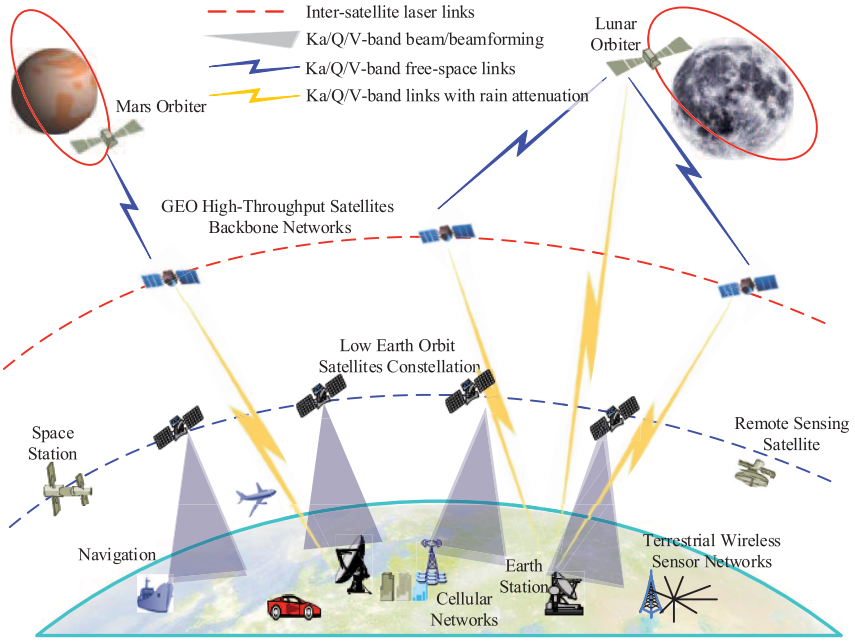

FIGURE 1. The architecture of future high-throughput integrated satellite-terrestrial networks.

(NAK) mechanism [16], [17], and the space nodes can obtain the delayed channel state information (CSI).

Therefore, in order to ensure a certain reliability in the performance of the Ka-band HTS communications, one needs to consider the tradeoffs between transmission latency, reliability, and onboard power allocations for the HTS nodes [18]. Wang *et al.* [19] designed a simple estimation scheme of CSI over the Ka-band channel with a delayed-feedback ACK/NAK message. For that, a transmit power allocation scheme can be proposed that maximizes the long-term throughput [20].

Hence, a rain attenuation prediction model to deal with a time-varying channel state is needed, and the Markov state model could be used to describe the Ka-band mmWave link state [21]. It is important to design a forecast algorithm based on the N-state Markov model to predict the weather state for the code-rate adaption on the sender side.

Moreover, with the estimation scheme of CSI, the space nodes can choose the appropriate code rate channel codes to enhance the transmission performance. Considering the CCSDS long erasure code (LEC) recommendation [22], and existing related rateless coding schemes [23], [24], approaching-capacity rateless codes with linear complexity represent a more suitable scheme for the integrated satellite-terrestrial networks with large-capacity data and multi-hop transmissions [25], [26] than the existing polar codes [27], spinal codes, Low-Density Parity-Check (LDPC) codes, and turbo codes.

In this paper, we choose the autoregressive moving-average (ARMA) model [28] to design our forecasting algorithm in Section II. This model can predict the N-state Markov chain of rain attenuation on the Ka-band link as the yellow links in Fig. 1, for which the prediction error may approach zero. In Section III, we propose an adaptive coding transmission (ACT) scheme over the Ka-band channel based on the analog fountain code (AFC), which is a rateless code that combines the Luby Transform (LT) code with m-ary modulation [29]. The proposed ACT scheme can approach the Shannon limit over a wide signal-to-noise ratio (SNR) range. In Section IV, we analysis the ACT scheme based on the ARMA prediction model for the Ka-band link in the integrated satellite-terrestrial networks as shown in Fig. 1. In Section V, we show through simulations that the proposed ACT scheme can increase system throughput and improve transmission efficiency. Finally, conclusions are drawn in Section VI.

II. N-STATE MARKOV MODEL AND FORECASTING

A. PRELIMINARIES OF THE ARMA MODEL

In this section, we design an N-state Markov chain to model the rain attenuation variation at Ka-band channel. We set the length of the transmission time slot is 90 seconds, and we choose a 3 seconds sample interval due to the round trip time of the Moon-to-Earth is about 2.64 seconds. Therefore, we need to sample 30 times in each time slot and use the average value to model the Markov channel. Moreover, due to the huge distance and long propagation delay in the integrated satellite-terrestrial networks, the transmitter can only obtain delayed CSI from feedback. Therefore, in this paper, our transmission system model adopts 1 time slot feedback CSI to design a practical time-varying rain attenuation prediction model based on the ARMA model for the integrated satellite-terrestrial networks.

In our previous work [30], we used the Van de Kamp (VDK) distribution-based model to design an N-state Markov chain. In this paper, by using the relationship

between the fade-slope standard deviation [28] and attenuation level [31] from fade-slope statistics of rain attenuation measured from Xi'an, China on March 14, 2010, we use the recommended statistical model in the International Telecommunication Union (ITU) standards to design an N-state Markov chain to generate the rain attenuation time series x_t, which can simulate a given duration rainfall event to help us design and verify the ARMA prediction algorithm.

Our channel estimation algorithm is designed by utilizing the ARMA model. In the $ARMA(p, q)$ model, p is the order of the autoregressive (AR) part $AR(p)$, and q is the order of the moving average (MA) part $MA(q)$. The $AR(p)$ part is used to predict the future value, which is only related to its previous predicted values, thus,

$$AR(p) : x_t = \sum_{i=1}^{p} \phi_i x_{t-i} + \varepsilon_t, \tag{1}$$

where $\phi_1, \phi_2, \ldots, \phi_p$ are the parameters of the $AR(p)$ model, and ε_t is white noise. The $MA(q)$ part is used to calculate the current accumulative errors of the predicted values by the $AR(p)$ part, where

$$MA(q) : x_t = \varepsilon_t + \sum_{i=1}^{q} \theta_i \varepsilon_{t-i}. \tag{2}$$

$\theta_1, \theta_2, \ldots, \theta_q$ are the parameters of the $MA(q)$ model, and ε_t is white noise.

Hence, the $ARMA(p, q)$ model is established by combining the above two parts and is given as follows:

$$ARMA(p, q) : x_t = \sum_{i=1}^{p} \phi_i x_{t-i} + \sum_{i=1}^{q} \theta_i \varepsilon_{t-i} + \varepsilon_t, \tag{3}$$

where ε_t is white noise which follows a normal distribution $N(0, \sigma^2)$ with zero mean and variance σ^2.

B. KEY PARAMETERS OF THE PROPOSED ARMA MODEL

The key to establish our rain attenuation prediction $ARMA(p, q)$ model is the course of estimating and solving the parameters in Equation (3). These parameters are closely related to the autocorrelation function (ACF) $\widehat{\rho}_k$ and the partial autocorrelation function (PACF) $\widehat{\varphi}_{k,k}$ of sequence x_t. $\widehat{\rho}_k$ and $\widehat{\varphi}_{k,k}$ indicate the trends and characteristics, respectively, of the primary data x_t. Thus, the first step of establishing a rain attenuation forecasting $ARMA(p, q)$ model is to obtain the $\widehat{\rho}_k$ and $\widehat{\varphi}_{k,k}$ of sequence x_t.

On one hand, the ACF $\widehat{\rho}_k$ shows the overall correlation of x_t and x_{t-k}, and the equation is given as follows:

$$\widehat{\rho}_k = \frac{\mathrm{cov}(x_t, x_{t-k})}{\sigma^2} = \frac{\mathrm{E}(x_t x_{t-k}) - \mathrm{E}(x_t)\mathrm{E}(x_{t-k})}{\sigma^2}. \tag{4}$$

On the other hand, the PACF $\widehat{\varphi}_{k,k}$ shows the immediate data dependency of x_t and x_{t-k} after removing all indirect correlations brought by the intermediate variables $x_{t-1}, x_{t-2}, \ldots, x_{t-k+1}$. By using the Yule Walker equation, the PACF $\widehat{\varphi}_{k,k}$ can be easily simplified as follows. First, for $j = 1, 2, \ldots, k$, we have

$$\begin{aligned} \widehat{\rho}_j &= \widehat{\rho}_{j-1}\widehat{\varphi}_{k,1} + \widehat{\rho}_{j-2}\widehat{\varphi}_{k,2} + \cdots + \widehat{\rho}_{j-k}\widehat{\varphi}_{k,k}, \\ &= \sum_{r=1}^{k} \widehat{\rho}_{j-r}\widehat{\varphi}_{k,r}, \end{aligned} \tag{5}$$

and $\widehat{\rho}_j = \widehat{\rho}_{-j}$. Then, the set of $\widehat{\rho}_j$ in Equation (5) can be solved by representing these equations in the matrix form with $j > 0$ and $\widehat{\rho}_0 = 1$. Thus Equation (5) is turned to

$$\begin{pmatrix} \widehat{\rho}_1 \\ \widehat{\rho}_2 \\ \cdots \\ \widehat{\rho}_k \end{pmatrix} = \begin{pmatrix} 1 & \widehat{\rho}_1 & \cdots & \widehat{\rho}_{k-1} \\ \widehat{\rho}_1 & 1 & \cdots & \widehat{\rho}_{k-2} \\ \cdots & \cdots & \cdots & \cdots \\ \widehat{\rho}_{k-1} & \widehat{\rho}_{k-2} & \cdots & 1 \end{pmatrix} \begin{pmatrix} \widehat{\varphi}_{k,1} \\ \widehat{\varphi}_{k,2} \\ \cdots \\ \widehat{\varphi}_{k,k} \end{pmatrix}. \tag{6}$$

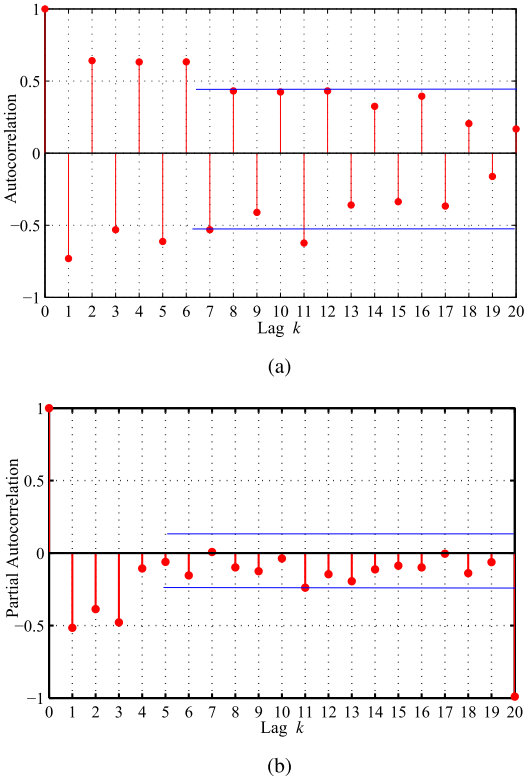

FIGURE 2. The calculation result of (a) the ACF and (b) the PACF.

Fig. 2 shows the values of ACF $\widehat{\rho}_k$ and PACF $\widehat{\varphi}_{k,k}$ corresponding to lag k, where lag is the number of afterward time windows and the rain attenuation series are generated from the N-state Markov chain. By the characteristics of these two value series, we can initially determine the order of the $ARMA(p, q)$ model according to the principles in [30]. The characteristics of the two value series can be indicated by truncation, which is a situation where the time series will be zero after several lags.

From Fig. 2(b), we can see that the value series of PACF $\widehat{\varphi}_{k,k}$ is truncated temporarily at lag $k = 5$, which means that the PACF $\widehat{\varphi}_{k,k}$ value is almost equal to 0 when lag $k = 5$ and

the PACF $\widehat{\varphi}_{k,k}$ value is close to 0 with $Lag > 5$. However, the ACF $\widehat{\rho}_k$ value is oscillatory, as shown in Fig. 2(a), and we can see that the value series of ACF $\widehat{\rho}_k$ is not truncated. In this case, as the the ACF $\widehat{\rho}_k$ value series are decreased after lag $k > 5$, we choose the lag $k = 6$ as a preliminary selection.

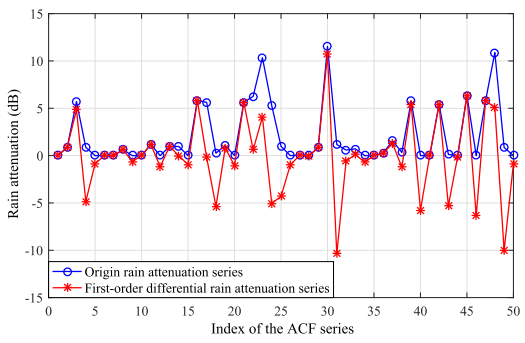

(a)

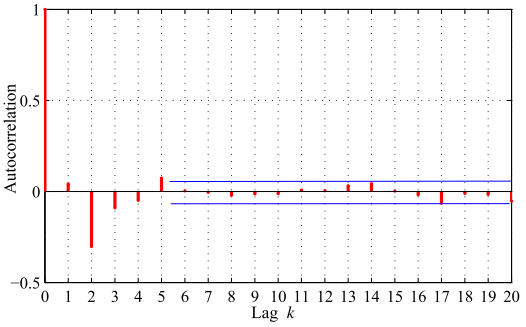

(b)

FIGURE 3. The improved (a) Rain attenuation series and (b) its first-order differential.

Furthermore, we can verify our preliminary selection for the ACF by using the first order of the differential equation, and an example of the improved ACF series to remove the oscillatory by using the first order differential equation is shown in Fig. 3. The ACF of the first-order differential rain attenuation series shown in Fig. 3(b) verifies that, if the selected order of ACF is correct, the $\widehat{\rho}_k$ value series will be truncated after the original rain attenuation series is processed by the first order differential equation.

Therefore, if the ACF $\widehat{\rho}_k$ and PACF $\widehat{\varphi}_{k,k}$ value series are truncated by lag $k_1 = 6$ and $k_2 = 5$, we can calculate the order of $ARMA(p, q)$ from $p = k_1 - k_2$, $q = k_1$. The result of the order for our $ARMA(p, q)$ model is: $p = 1$, $q = 6$. Therefore, we can substitute the original data series x_t into the $ARMA(1, 6)$ model as follows:

$$ARMA(1,6): x_t = \phi_1 x_{t-1} + \theta_1 \varepsilon_{t-1} + \cdots + \theta_6 \varepsilon_{t-6} + \varepsilon_t, \quad (7)$$

where ε_t is normal distribution $N(0, \sigma^2)$ with zero mean and variance σ^2.

C. CALCULATION METHOD OF THE COEFFICIENTS FOR THE PROPOSED ARMA(1, 6) MODEL

Then, to calculate the rest coefficients ϕ_k, θ_k and σ^2 in the $ARMA(1, 6)$ model, such as those left in Equation (3), once again, we **solve** ϕ_k by utilizing the YuleâĂ"Walker equation in a simple way. Thus,

$$\begin{pmatrix} \phi_1 \\ \phi_2 \\ \cdots \\ \phi_p \end{pmatrix} = \begin{pmatrix} \gamma_q & \gamma_{q-1} & \cdots & \gamma_{q-p+1} \\ \gamma_{q+1} & \gamma_q & \cdots & \gamma_{q-p+2} \\ \cdots & \cdots & \cdots & \cdots \\ \gamma_{q+p-1} & \gamma_{q+p-2} & \cdots & \gamma_q \end{pmatrix}^{-1} \begin{pmatrix} \gamma_{q+1} \\ \gamma_{q+2} \\ \cdots \\ \gamma_{q+p} \end{pmatrix}. \quad (8)$$

Therefore, we have p coefficients as $\phi_{k\in\{1,2,\ldots,p\}}$, where γ_k is autocovariance function of the ARMA model, and $\gamma_k = E(x_t\, x_{t-k})$, for $k \in \{0, 1, \ldots, p\}$, and we **solve** θ_k as follows:

$$\begin{cases} \gamma_0 = \sigma^2(\theta_0\theta_0 + \theta_1\theta_1 + \cdots + \theta_q\theta_q) \\ \gamma_1 = \sigma^2(\theta_0\theta_1 + \theta_1\theta_2 + \cdots + \theta_{q-1}\theta_q) \\ \cdots \\ \gamma_k = \sigma^2(\theta_0\theta_k + \theta_1\theta_{1+k} + \cdots + \theta_{q-k}\theta_q) \\ \cdots \\ \gamma_q = \sigma^2(\theta_0\theta_q + \theta_1\theta_{1+q} + \cdots + \theta_0\theta_q) \end{cases} \quad (9)$$

There are $q + 1$ equations in (9), where q undetermined coefficients $\theta_{k\in\{1,2,\ldots,p\}}$, and one unknown parameter σ^2. In our $ARMA(1, 6)$ model, $p = 1$, $q = 6$, $\phi_1 = \gamma_7/\gamma_6$ and $\theta_0 = 1$. To calculate these numerical results from the nonlinear equations (9), we can utilize several linear iteration algorithms, such as the Newton-Raphson algorithm. In this paper, we use the same N-state Markov channel to generate four rainfall events where the maximum rain fading is 10 dB. Then, we use the ARMAX function in Matlab to calculate the coefficients of our $ARMA(1, 6)$ model, and the results of the coefficient values are shown in Table 1.

TABLE 1. Coefficient results of different serials in ARMA(1, 6).

Parameter	Serial 1	Serial 2	Serial 3	Serial 4
ϕ_1	0.848	–0.530	0.577	0.560
θ_1	0.027	–1.685	–0.205	–0.268
θ_2	–0.431	0.907	–0.391	–0.271
θ_3	–0.078	–0.308	–0.147	–0.101
θ_4	0.034	0.299	–0.121	0.012
θ_5	0.220	–0.219	0.00004	–0.109
θ_6	–0.020	0.043	–0.136	0.338

Then, we can adopt the four data series shown in Table 1 as the initial input to generate the N-state Markov chain. As the length of the Markov chain sequences is set as 50, we can obtain the four sequences which correspond to their respective estimation parameters by using the $ARMA(1, 6)$ model. To analyze each set of the previous 25 pilots of each sequence, we have

$$x_t = 0.848x_{t-1} + \varepsilon_t + 0.027\varepsilon_{t-1} - 0.431\varepsilon_{t-2} - 0.078\varepsilon_{t-3} + 0.034\varepsilon_{t-4} + 0.22\varepsilon_{t-5} - 0.02\varepsilon_{t-6}. \quad (10)$$

We can use the latest 25 data values as pilots, and then compare them to the upcoming 25 data values in order to

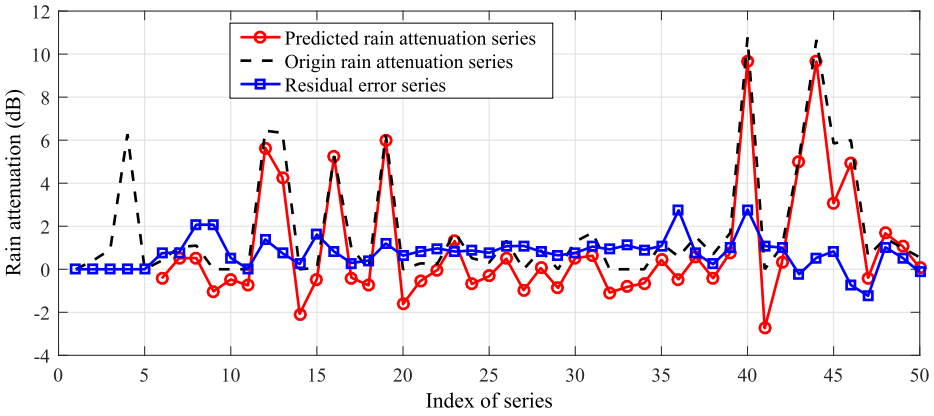

FIGURE 4. Comparison of the prediction values and the original value.

measure the prediction accuracy of our $ARMA(1, 6)$ model. The estimation error simulation result of the first sequence in Table 1 is shown in Fig. 4, and the corresponding ACFs and PACFs of the first-order differential rain attenuation series are shown in Fig. 5.

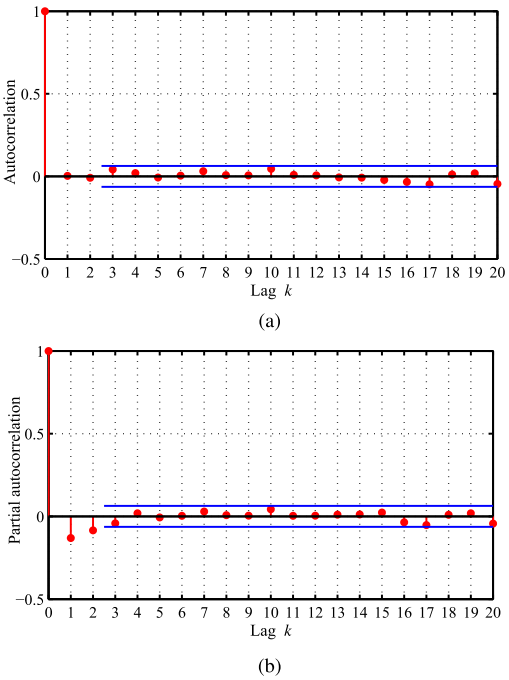

FIGURE 5. (a) The ACF and (b) PACF of the first-order differential rain attenuation.

In general, quantization of the veracity of forecast results firstly includes the absolute error of predicted points, which is the difference between the predicted values and actual values. It has the same order as the prediction data. Secondly, the relative error of predicted points is included, which is the ratio of the deviation and the actual results. There is a difference in the deviation between the predicted results and actual results, the relative error has no unit and is usually expressed as a percentage. We use the mean absolute error to measure the prediction error. When the rain attenuation fading depth is 10 dB, the average prediction error is 0.0227 dB when using our $ARMA(1, 6)$ model with respect to the N-state Markov chain, taking the mean absolute errors. We will verify the performance of our $ARMA(1, 6)$ prediction model later in Section V.

III. ANALOG FOUNTAIN CODES AND OPTIMIZATION

Moreover, the conventional channel codes with fixed code-rate and the block length are unable to meet the time-varying N-state wireless communication channel capacity at all times [32], especially if the duration of each channel state in Ka-band channel is very short (i.e., several seconds or minutes). When the rate is larger than the capacity, transmissions are said to unreliable [33], and when the rate is smaller than the capacity, transmissions are said to be inefficient.

Alternatively, when CSI is known a priori at the transmitter side, adaptive coded modulation (ACM) can be used [34]. However, ACM can only obtain a step-like throughput. In this section, we consider a rateless code known as the AFC for which the CSI is not needed at the transmitter. Instead, the rate is determined on the fly and, thus, achieves a seamless performance across all channel states.

A. AFC ENCODER

The adaptive coding modulation (ACM) is proposed to enhance the transmission efficiency over the time-varying wireless channels. Recently, Shirvanimoghaddam *et al.* [29] proposed the AFC scheme, which is a combination of the binary fountain code (FC) with the idea behind m-ary modulation. For this, the information bits are first modulated using binary phase-shift keying (BPSK).

In a manner similar to binary FCs, AFCs can be represented in the form of a bipartite graph as shown in Fig. 6. In Fig. 6, the circles represent the information symbols $[b_i]_{i=1,2,\ldots,k}$. They are commonly referred to as variable nodes. The squares represent the coded symbols $[S_j]_{j=1,2,\ldots,N}$ and are commonly referred to as check nodes.

First, a positive integer d is chosen from a predetermined distribution $\Omega(x) = \sum_d \Omega_d x^d$, where d is commonly referred to as the degree, and Ω_d is the corresponding degree

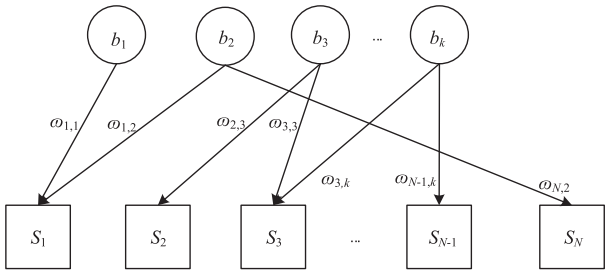

FIGURE 6. Analog fountain code (AFC) encoding scheme.

probability. Then, d information symbols are chosen uniformly at random and multiplied by d coefficients chosen uniformly at random from a predetermined set w_s. Finally, the coded symbol is the sum of these weighted symbols. In particular, the j^{th} coded symbol S_j can be expressed as

$$S_j = \sum_{i=1}^{d_j} w_{j,i} b_i, \tag{11}$$

where d_j is the chosen degree, and $w_{j,i}$ are the randomly selected weights from the set w_s.

Therefore, the binary elements "1" in conventional LT codes generator matrix $\boldsymbol{G}$ are replaced by the corresponding real weights $w_{j,i}$ in the AFC generator matrix.

Intuitively, the performance of AFC is dependent on the proper design of the degree distribution $\Omega(x)$ and the weight set w_s [35]. From the Shannon limit, these two parameters need to be designed such that the stream of coded symbols follows a Gaussian-like distribution.

Hence, both the degree distribution and weight set can affect the performance of the AFC scheme. On one hand, the optimization of the degree distribution is used to find out the optimization condition via And-Or tree analysis, and then solve the optimal results by utilizing linear programming [36]. In the previous study [37], we found out that the degree distribution of the AFC scheme is not the main factor with respect to the decoding performance. In contrast, in the finite block length regime, a constant degree distribution is preferred, e.g., all the AFC coded nodes $[S_j]_{j=1,2,...,N}$ are with $\Omega(x) = x^8$ as in the practical application, without considering the unequal error protection [38], [39].

B. WEIGHT SET OPTIMIZATION

On the other hand, the design of the AFC weight set is important, an optimum selection weight set can improve the decoding performance. An optimum weight set is that which leads to the weight distribution of the received coded symbols closer to the Gaussian distribution, e.g., the AFC with weight set $\{\pm4, \pm3, \pm2, \pm1\}$ has a better decoding performance than with the weight set $\{\pm4, \pm4, \pm2, \pm1\}$ [36].

C. AFC DECODER

In this paper, considering the huge noise and frequent interruptions of the Ka-band GEO satellites relaying communications in the the integrated satellite-terrestrial backbone network, we chose the compression perception belief propagation (CSBP) decoding algorithm to enhance the decoding performance. The algorithm is detailed in [40]. By using the CSBP decoding algorithm, and choosing degree distribution $\Omega(x) = x^8$ and the weight set $w_s = \{\pm4, \pm3, \pm2, \pm1\}$, we will compare the decoding performance with different block lengths and code-rates. Furthermore, we compared the decoding performance with the LDPC codes in [41], where the number of variable nodes is $k = 100$, and the code-rate of the LDPC codes are 0.95, 0.8 and 0.6, respectively.

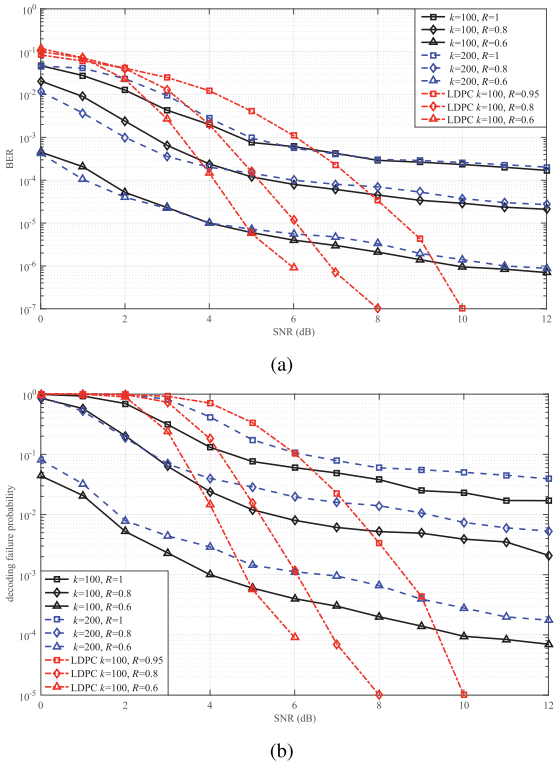

FIGURE 7. Decoding performance of AFC and LDPC codes: (a) BER; (b) DFP.

The simulation results of the decoding failure probability versus SNR are shown in Fig. 7(a), where the number of variable nodes in the AFC scheme is $k = 100, 200$, and the code-rate is $R = k/n = \{1, 0.8, 0.6\}$. When $R = 1$, the bit error rate (BER) of the AFC with $k = 100, 200$ is about 10^{-3} orders of magnitude when the $SNR \geq 10$ dB. When $R = 0.6$, the BER of the AFC is decreased to 10^{-5} when the $SNR \geq 5$ dB, and the BER can decrease to 10^{-6} when the $SNR \geq 10$ dB.

As shown in Fig. 7, the AFC schemes have error floor problems compared to the LDPC codes. The LDPC code with lower code-rate can achieve a very low error floor if the SNR is larger than its decoding threshold value. However, the achievable rate of the fixed rate LDPC codes can perform well only in a small range of SNRs.

Fig. 8 shows the achievable rate of the AFC schemes and LDPC codes from DVB-S2 [41] with different rate and

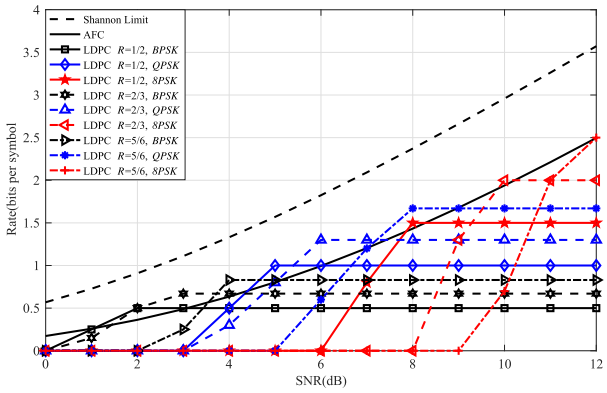

FIGURE 8. Achievable rate of the AFC schemes and the LDPC codes versus signal-to-noise ratios (SNRs) for $BER = 10^{-4}$.

modulation types in the AWGN channel, versus the SNR for $BER = 10^{-4}$. Clearly, the maximum achievable rate of AFC scheme outperforms the LDPC codes in the simulation range of SNRs. It is important to note that the fixed rate LDPC codes can be optimized for a specific SNR, however, they are not optimal for other SNRs.

IV. ADAPTIVE CODING TRANSMISSION SCHEME BASED ON THE ARMA (1, 6) MODEL

A. DESIGN OF THE ADAPTIVE CODING TRANSMISSION SCHEME

We assume a Ka-band GEO satellites relaying the communication link can be divided into discrete transmission time windows with constant duration, and the rain attenuation is modeled by the N-state Markov chain. Without loss of generality, we select a constant duration of each time window (90 seconds) and a transmission data rate (20kB/s), and then the number n of the coded symbols can be transmitted in a time window is determined.

According to the Markov theory, assuming that the stationary distribution of N states is $\vec{P} = (P^1, P^2, \ldots, P^N)$, then $\vec{P} = \vec{P}Q$, where Q is the matrix of transition probability of the Markov chain, and $P^1 + P^2 + \cdots + P^N = 1$. Moreover, we assume p_i is the BER of the ith state in the N-state Markov chain and $p_1 \leq p_2 \leq \ldots \leq p_i \leq \ldots \leq p_N$. Let L denotes the length of the coded symbol, and P_i denotes the symbol loss probability in the ith Markov state, we have

$$P_i = 1 - (1 - p_i)^L. \tag{12}$$

Then, let n_i and k_i denote the expected number of the received coded symbols and the recovery information symbols in a transmission time window in the ith Markov state, respectively. The relationship between the number of the transmitted symbols n and the received symbols n_i is

$$n_i = (1 - P_i) \cdot n, \tag{13}$$

and the overhead O_i of the ith Markov state in a transmission time window can be calculated as

$$O_i = \frac{n - k_i}{k_i}. \tag{14}$$

Therefore, in our ACT scheme, the sender can predict the weather state and then adaptively select the applicable coding overhead according to the $ARMA(1, 6)$ prediction result and Equation (14). Hence, for the N-state Markov chain with the stationary distribution of N states $P^1 \leq P^2 \leq \ldots \leq P^N$, the average coding overhead of the ACT scheme for the N-state Markov channel is

$$O_a = \frac{n - \sum_{i=1}^{N} P^i k_i}{\sum_{i=1}^{N} P^i k_i}. \tag{15}$$

Let F_e denotes the average prediction error of our $ARMA(1, 6)$ model. From the above assumption and analysis, if the sender predicts the next transmission time window is in the 1st Markov state (i.e., the worst state), then the expected recovery information symbols in the next transmission time window is k_1. If the sender predicts the next transmission time window is in the 2nd Markov state, then the expected recovery information symbols in the next transmission time window is $k_2(1 - F_e/N)$. If the sender predicts the next transmission time window is in the 3rd Markov state, then the expected recovery information symbols in the next transmission time window is $k_3(1 - 2F_e/N)$. Therefore, the throughput G of the ACT scheme can be calculated as follows

$$G = P^1 k_1 + \sum_{i=2}^{N} k_i (P^i - \frac{(i-1)F_e}{N}). \tag{16}$$

In contrast, if the sender chooses to transmit with a fixed overhead, such as the ith Markov state overhead, the throughput of the fixed scheme can be modeled as

$$\begin{cases} G_1 = k_1, \\ G_i = k_i \cdot (1 - \sum_{j=1}^{i-1} P^j), \quad \text{for} \quad i > 1. \end{cases} \tag{17}$$

This can help the space nodes in the integrated satellite-terrestrial networks tradeoffs between reliability and limited communication resources.

B. COMPLEXITY ANALYSIS OF AFC IN THE ADAPTIVE CODING TRANSMISSION SCHEME

The complexity of our ACT scheme is an important factor for determining the corresponding coding parameters of the AFC for the integrated satellite-terrestrial network communications. We consider the AFC with k variable nodes, and assume the corresponding generated matrix $\boldsymbol{G}$, for which the maximum number of nonzero elements in each column and row is C and R, respectively. The complexity of generating $\boldsymbol{G}$ is $O(C \cdot k)$. Moreover, each encoded node is connected with at most R variable nodes. Then, the table size is 2^R for every encoded node, and the complexity of the AFC with block length n AFC is $O(n)$. On the decoder side, we adopt the CSBP decoding algorithm which is a kind of updated belief propagation (BP) algorithm. In each iteration decoding round, the maximum computation complexity is $O(C \cdot \mathcal{W})$, which is a constant and $\mathcal{W} = 1 + \sum_{i=1}^{R} \mid w_i \mid$. Therefore, the total computation complexity of the CSBP algorithm is $O(C \cdot k \cdot \mathcal{W})$. In a well-designed AFC scheme, $\mathcal{W}$ and C are

both constant, and the AFC scheme can be considered to have linear computation complexity.

V. SIMULATIONS AND DISCUSSION

A. PREDICTION ERROR ANALYSIS OF THE ARMA (1, 6) MODEL

We first present the Monte Carlo simulation results to evaluate the performance of our *ARMA*(1, 6) prediction model. Moreover, consider that the sender can obtain the delayed CSI by NAK feedback in the integrated satellite-terrestrial network communications, and it can use the feedback channel states of the last-n time windows to enhance the prediction error of the *ARMA*(1, 6) prediction model. However, the tradeoffs between reliability, computational complexity and buffer consumptions should be considered.

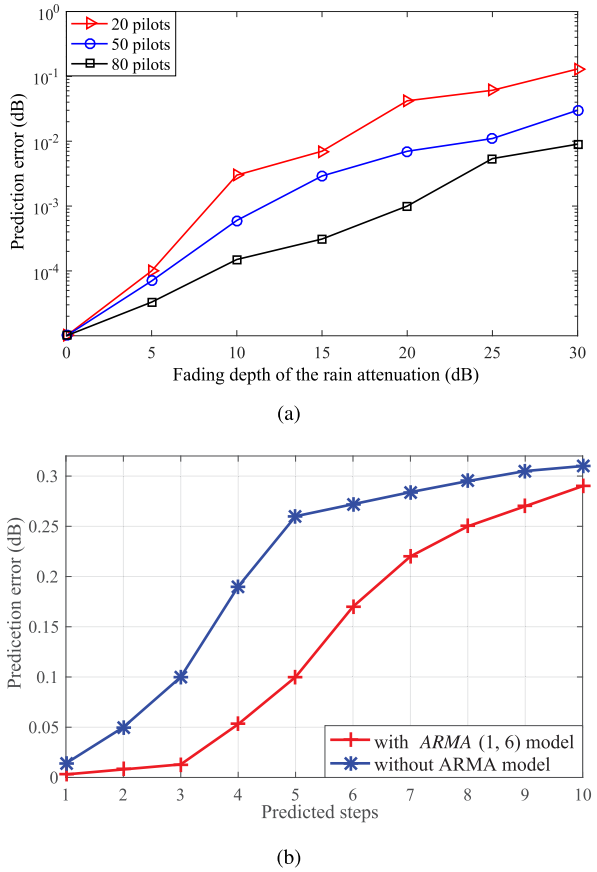

FIGURE 9. Impact of the autoregressive moving-average (ARMA) model estimation to the ACT scheme: (a) different number of the pilots; (b) prediction error.

Fig. 9(a) shows the one-step prediction error of our *ARMA*(1, 6) model with a five-state Markov chain for seven different rain attenuation SNR values: 0 dB, 5 dB, 10 dB, 15 dB, 20 dB, 25 dB, and 30 dB. Each simulation data point is running 1000 times. Obviously, as the number of the pilots is increased from 20 to 80, the prediction result became more precise. Considering the tradeoffs between reliability, computational complexity and buffer consumptions, we selected 25 pilots and 10 dB rain attenuation. The prediction errors versus predicted steps are shown in Fig. 9(b). The prediction error slowly increases with the predicted steps, which indicates that our *ARMA*(1, 6) model can perform well in the case the sender can not receive channel state feedback in a short time.

B. CHANNEL ESTIMATION AFFECTION IN THE ADAPTIVE CODING TRANSMISSION SCHEME

Based on the above discussion, considering the prediction error in our *ARMA*(1, 6) model, in this subsection we simulate the mean absolute errors with the prediction error.

Assuming the number of variable nodes k is 100, the simulation result of the decoding failure probability with a error range from -2 dB to 2 dB on the different rain attenuation SNR values 10 dB, 15 dB, 20 dB, and 25 dB are shown in Fig. 10. Each simulation data point runs 1000 times. As shown in Fig. 10, the estimation error has little effect on the the decoding performance of the ACT scheme if our *ARMA*(1, 6) model can limit the rain attenuation prediction error in ± 2 dB, which can be achieved in the most situations.

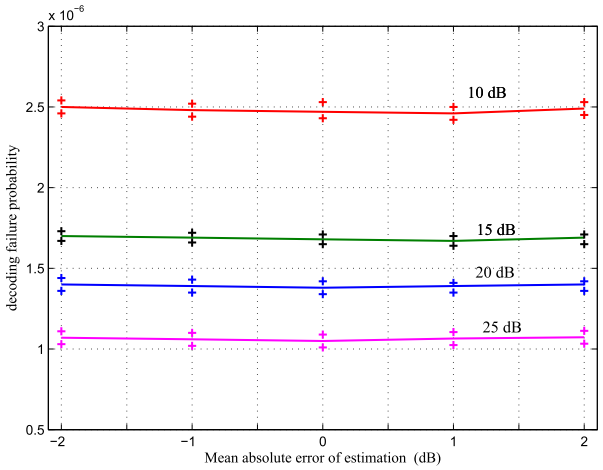

FIGURE 10. Impact of different signal-to-noise ratios (SNRs) on the adaptive coding transmission scheme.

C. PERFORMANCE OF THE ADAPTIVE CODING TRANSMISSION SCHEME

In this subsection, we simulate the performance of our ACT scheme. According to the record of the rain attenuation in Xi'an, China on March 14, 2010, where the rain attenuation fading depth was 8 dB, we select four-state rain fading with 0 dB, 4 dB, 6 dB, and 8 dB. Therefore, a four-state Markov chain can be modeled [28], and the corresponding Markov transition matrix is given as follows:

$$\mathbf{P} = \begin{pmatrix} 0.9986 & 0.0014 & 0.0000 & 0.0000 \\ 0.0007 & 0.9986 & 0.0007 & 0.0000 \\ 0.0000 & 0.0007 & 0.9986 & 0.0007 \\ 0.0000 & 0.0000 & 0.0014 & 0.9986 \end{pmatrix}. \quad (18)$$

According to the Markov random process theory, the stationary probability of each state is $P^1 = 0.1667$, $P^2 = 0.3333$, $P^3 = 0.3333$, $P^4 = 0.1667$. We simulate

TABLE 2. Simulation parameters. LT: Luby Transform.

Parameter	Values
Transmission power	32 W
Data rate	20kB/s
Time window duration	90 s
Prediction error	0.0227 dB
BER corresponding to the four-state Ka-band channel	$10^{-3}, 10^{-4}, 10^{-6}, 10^{-14}$
Overhead of the ACT scheme	$0.67, 0.25, 0, 0$
Overhead of the fixed scheme	$0.67, 0.25, 0, 0$
Overhead of the adaptive LT coding scheme [23]	$5.17, 2.97, 0.463, 0.45$

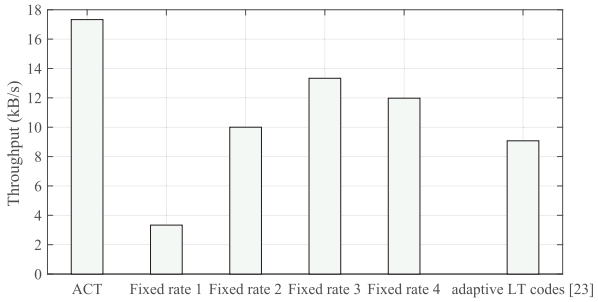

FIGURE 11. Throughput simulation of different coding schemes.

the performance of our ACT scheme and compare it with corresponding fixed rate coding scheme and the adaptive LT coding scheme in [23]. The system parameters are provided in Table 2.

The Ka-band link communication parameters are selected from the typical the integrated satellite-terrestrial network communications, which are referred from [6]. The transmission power is 32 W, we can assume that $SNR_0 = 15$ dB is the case without channel fading. Corresponding to the selected four rain attenuation values, we can obtain four channel states: $SNR_1 = 7$ dB, $SNR_2 = 9$ dB, $SNR_3 = 11$ dB, and $SNR_4 = 15$ dB. By using BPSK modulation, we derived the relation of the BER and SNR as follows

$$P_{eDPSK} = \frac{1}{2}\exp(-SNR). \tag{19}$$

Accordingly, we have four BERs which correspond to the four states: $p_1 = 3.3 \times 10^{-3}$, $p_2 = 1.7 \times 10^{-4}$, $p_3 = 1.7 \times 10^{-6}$, and $p_4 = 9.2 \times 10^{-15}$. In this simulation, the communication link is modeled by a four-state Markov chain; we keep the receiver decoding failure probability less than 10^{-6} and calculate the code-rate in Table 2.

Then, we compare our ACT scheme with the four fixed-rate schemes and adaptive LT coding scheme. The simulation result is shown in Fig. 11. The decoding overhead of the first fixed scheme is 0.67, that of the second fixed scheme is 0.25, and the third and fourth fixed schemes have fixed overheads 0 each of them, they correspond to the channel state BERs of 10^{-3}, 10^{-4}, 10^{-6}, 10^{-14}, respectively. As shown in Fig. 11, the throughput performance results of the four fixed-rate schemes are related not only to the code-rate, but also are related to the channel states. We find that the throughput of the proposed ACT scheme is over 15% greater than for the fixed rate schemes and the adaptive LT coding scheme.

VI. CONCLUSION

In this paper, we analyzed the rain attenuation of the Ka-band channel and modeled an N-state Markov channel to capture a channel capacity that randomly ranged from a good to bad state for future integrated satellite-terrestrial network communications. Then, by using the ARMA model, we proposed the practical time-varying rain attenuation prediction algorithm $ARMA(1, 6)$ model for the modeled N-state Markov chain channel, which can reduce the prediction error probability to an error range of about 0.0027 dB error in a 10 dB rain attenuation fading depth. Moreover, by analyzing the overhead of the AFC schemes under certain decoding failure probabilities corresponding to the predicted SNR from our $ARMA(1, 6)$ prediction model, we designed an ACT scheme based on the AFC coding scheme, and the key parameters of AFC were selected based on a tradeoff between decoding failure probability, block length, and maximal code-rate for the integrated satellite-terrestrial network communications. Simulation results show that our proposed scheme can effectively improve throughput and efficiency with respect to existing fixed-rate coding schemes.

ACKNOWLEDGMENT

Shushi Gu, Zixuan Huang, and Shaohua Wu contributed equally to this work.

REFERENCES

[1] M. Jia, X. Gu, Q. Guo, W. Xiang, and N. Zhang, "Broadband hybrid satellite-terrestrial communication systems based on cognitive radio toward 5G," *IEEE Wireless Commun.*, vol. 23, no. 6, pp. 96–106, Dec. 2016.

[2] J. Jiao, H. Gao, S. Wu, and Q. Zhang, "Performance analysis of space information networks with backbone satellite relaying for vehicular networks," *Wireless Commun. Mobile Comput.*, vol. 2017, Dec. 2017, Art. no. 4859835.

[3] J. Jiao, Y. Hu, Q. Zhang, and S. Wu, "Performance modeling of LTP-HARQ schemes over OSTBC-MIMO channels for hybrid satellite terrestrial networks," *IEEE Access*, vol. 6, pp. 5256–5268, 2018.

[4] D. Bell *et al.*, "MRO relay telecom support of Mars Science Laboratory surface operations," in *Proc. IEEE Aerosp. Conf.*, Big Sky, MT, USA, Mar. 2014, pp. 1–10.

[5] *Recommendations a Strategy for Space Internetworking*, document SISG Report v1.4,, Nov. 2008. [Online]. Available: https://cwe.ccsds.org/ioag/Final Products/SISG Reportv1.4 FINAL.pdf

[6] I. U. Sung and J. L. Gao, "CFDP performance over weather-dependent Ka-band channel," in *Proc. Amer. Inst. Aeronaut. Astronaut. Conf.*, Rome, Italy, 2006, pp. 1–21.

[7] N. Adams, D. Copeland, A. Mick, and N. Pinkine, "Optimization of deep-space Ka-band link schedules," in *Proc. IEEE Aerosp. Conf.*, Big Sky, MT, USA, Mar. 2014, pp. 1–7.

[8] S. Maleki *et al.*, "Cognitive spectrum utilization in Ka band multi-beam satellite communications," *IEEE Commun. Mag.*, vol. 53, no. 3, pp. 24–29, Mar. 2015.

[9] J. Jiao *et al.*, "Reliable deep-space file transfers: How data transfer can be ensured within a single round-trip interval," *IEEE Veh. Technol. Mag.*, vol. 12, no. 4, pp. 86–94, Dec. 2017.

[10] J. L. Gao, "On the performance of adaptive data rate over deep space Ka-band link: Case study using kepler data," in *Proc. IEEE Aerosp. Conf.*, Big Sky, MT, USA, Mar. 2016, pp. 1–7.

[11] *Licklider Transmission Protocol (LTP) for CCSDS*, document CCSDS 734.1-B-1, CCSDS, May 2015. [Online]. Available: https://public.ccsds.org/Pubs/734x1b1.pdf

[12] P. V. R. Ferreira, R. Paffenroth, and A. M. Wyglinski, "Interactive multiple model filter for land-mobile satellite communications at Ka-band," *IEEE Access*, vol. 5, pp. 15414–15427, 2017.

[13] K. Zoltán, "Channel adaptive output back-off setting of non-linear power amplifiers for high throughput multi-spot beam satellite systems," *Int. J. Satellite Commun. Netw.*, vol. 33, no. 5, pp. 391–404, 2015.
[14] L. Shi *et al.*, "Integration of Reed–Solomon codes to licklider transmission protocol (LTP) for space DTN," *IEEE Aerosp. Electron. Syst. Mag.*, vol. 32, no. 4, pp. 48–55, Apr. 2017.
[15] R. Wang, M. Qiu, K. Zhao, and Y. Qian, "Optimal RTO timer for best transmission efficiency of DTN protocol in deep-space vehicle communications," *IEEE Trans. Veh. Technol.*, vol. 66, no. 3, pp. 2536–2550, Mar. 2017.
[16] *CCSDS File Delivery Protocol (CFDP)*, document CCSDS 727.0-B-4, Blue Book, Irvine, CA, USA, Jan. 2007. [Online]. Available: https://public.ccsds.org/Pubs/727x0b4.pdf
[17] Q. Yu *et al.*, "Modeling RTT for DTN protocol over asymmetric cislunar space channels," *IEEE Syst. J.*, vol. 10, no. 2, pp. 556–567, Jun. 2016.
[18] T. de Cola, E. Paolini, G. Liva, and G. P. Calzolari, "Reliability options for data communications in the future deep-space missions," *Proc. IEEE*, vol. 99, no. 11, pp. 2056–2074, Nov. 2011.
[19] G. Wang, S. C. Burleigh, R. Wang, L. Shi, and Y. Qian, "Scoping contact graph-routing scalability: Investigating the system's usability in space-vehicle communication networks," *IEEE Veh. Technol. Mag.*, vol. 11, no. 4, pp. 46–52, Dec. 2016.
[20] J. Jiao, X. Sui, S. Gu, S. Wu, and Q. Zhang, "Partially observable Markov decision process-based transmission policy over Ka-band channels for space information networks," *Entropy*, vol. 19, no. 10, p. 510, 2017.
[21] L. Castanet, T. Deloues, and J. Lemorton, "Channel modelling based on N-state Markov chains for satcom systems simulation," in *Proc. 25th Int. Conf. Antennas Propag. (ICAP)*, Exeter, U.K., Mar./Apr. 2003, pp. 119–122.
[22] *Erasure Correcting Codes for Use in Near-Earth and Deep-Space Communications*, document CCSDS 131.5-O-1, Orange Book, Houston, TX, USA, Nov. 2014. [Online]. Available: https://public.ccsds.org/Pubs/131x5o1.pdf
[23] J. Jiao, Q. Guol, and Q. Zhang, "Packets interleaving CCSDS file delivery protocol in deep space communication," *IEEE Aerosp. Electron. Syst. Mag.*, vol. 26, no. 2, pp. 5–11, Feb. 2011.
[24] K. Zhang, Q. Zhang, and J. Jiao, "Bounds on the reliability of RaptorQ codes in the finite-length regime," *IEEE Access*, vol. 5, pp. 24766–24774, 2017.
[25] J. Jiao, Y. Yang, B. Feng, S. Wu, Y. Li, and Q. Zhang, "Distributed rateless codes with unequal error protection property for space information networks," *Entropy*, vol. 19, no. 1, p. 38, 2017.
[26] S. Gu, J. Jiao, Q. Zhang, Z. Yang, W. Xiang, and B. Cao, "Network-coded rateless coding scheme in erasure multiple-access relay enable communications," *IET Commun.*, vol. 8, no. 4, pp. 537–545, Mar. 2014.
[27] B. Feng, Q. Zhang, and J. Jiao, "An efficient rateless scheme based on the extendibility of systematic polar codes," *IEEE Access*, vol. 5, pp. 23223–23232, 2017.
[28] *Propagation Data and Prediction Methods Required for the Design of Earth-Space Telecommunication Systems*, document ITU-R P.618–12, Geneva, Switzerland, 2015. [Online]. Available: www.srrc.org.cn/spreadmodel/PDFile/R-REC-P.618-12-201507-I!!PDF-E.pdf
[29] M. Shirvanimoghaddam, Y. Li, and B. Vucetic, "Near-capacity adaptive analog fountain codes for wireless channels," *IEEE Commun. Lett.*, vol. 17, no. 12, pp. 2241–2244, Dec. 2013.
[30] C. Chen, J. Jiao, H. Wu, Y. Li, and Q. Zhang, "Adaptive rateless coding scheme for deep-space Ka-band communications," in *Proc. IEEE Int. Conf. Wireless Space Extreme Environ. (WiSEE)*, Aachen, Germany, Sep. 2016, pp. 77–81.
[31] M. Van de Kamp, *Climatic Radiowave Propagation Models for the Design of Satellite Communication Systems*. Eindhoven, The Netherlands: Eindhoven Univ. Technol., 1999.
[32] M. Shojafar, N. Cordeschi, and E. Baccarelli, "Energy-efficient adaptive resource management for real-time vehicular cloud services," *IEEE Trans. Cloud Comput.*, to be published. [Online]. Available: https://ieeexplore.ieee.org/document/7448886/, doi: 10.1109/TCC.2016.2551747.
[33] X. Fan, L. Huang, Y. Huo, C. Hu, Y. Tian, and J. Qian, "Space power synthesis-based cooperative jamming for unknown channel state information," in *Proc. 12th Int. Conf. Wireless Algorithms, Syst., Appl. (WASA)*, Guilin, China, Jun. 2017, pp. 483–495.
[34] N. Cordeschi, D. Amendola, M. Shojafar, and E. Baccarelli, "Distributed and adaptive resource management in cloud-assisted cognitive radio vehicular networks with hard reliability guarantees," *Veh. Commun.*, vol. 2, no. 1, pp. 1–12, 2015.
[35] M. Shirvanimoghaddam, Y. Li, B. Vucetic, J. Yuan, and P. Zhang, "Binary compressive sensing via analog fountain coding," *IEEE Trans. Signal Process.*, vol. 63, no. 24, pp. 6540–6552, Dec. 2015.
[36] M. Shirvanimoghaddam, Y. Li, M. Dohler, B. Vucetic, and S. Feng, "Probabilistic rateless multiple access for machine-to-machine communication," *IEEE Trans. Wireless Commun.*, vol. 14, no. 12, pp. 6815–6826, Dec. 2015.
[37] R. Abbas, M. Shirvanimoghaddam, Y. Li, and B. Vucetic, "Random access for M2M communications with QoS guarantees," *IEEE Trans. Commun.*, vol. 65, no. 7, pp. 2889–2903, Jul. 2017.
[38] R. Abbas, M. Shirvanimoghaddam, Y. Li, and B. Vucetic, "Performance analysis and optimization of LT codes with unequal recovery time and intermediate feedback," in *Proc. IEEE Int. Conf. Commun. (ICC)*, Kuala Lumpur, Malaysia, May 2016, pp. 1–6.
[39] R. Abbas, M. Shirvanimoghaddam, Y. Li, and B. Vucetic, "Analysis on LT codes for unequal recovery time with complete and partial feedback," in *Proc. IEEE Int. Symp. Inf. Theory (ISIT)*, Barcelona, Spain, Jul. 2016, pp. 305–309.
[40] H. Cui, C. Luo, K. Tan, K. Wu, and C.-W. Chen, "Seamless rate adaptation for wireless networking," in *Proc. 14th Int. Symp. Modeling Anal. Simulation Wireless Mobile Syst.*, Miami, FL, USA, Oct. 2011, pp. 437–446.
[41] *Digital Video Broadcasting (DVB); Second Generation Framing Structure, Channel Coding and Modulation Systems for Broadcasting, Interactive Services, News Gathering and Other Broadband Satellite Applications (DVB-S2)*, document ETSI EN 302 307 (V1.2.1), ETSI, Aug. 2009. [Online]. Available: http://www.etsi.org/deliver/etsi_en

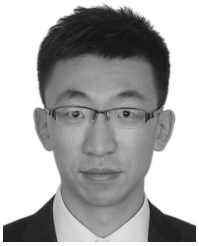

SHUSHI GU received the M.S and Ph.D. degrees in communication engineering from the Harbin Institute of Technology (HIT), Shenzhen, China, in 2012 and 2016, respectively. He is currently a Post-Doctoral Research Fellow with the Communication Engineering Research Centre, Shenzhen Graduate School, HIT. His current interests include erasure codes, network and channel coding, space information networks, and distributed storage system.

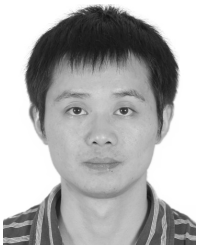

JIAN JIAO (M'16) received the M.S and Ph.D. degrees in communication engineering from the Harbin Institute of Technology (HIT), Shenzhen, China, in 2007 and 2011, respectively. From 2011 to 2015, he was a Post-Doctoral Research Fellow with the Communication Engineering Research Centre, Shenzhen Graduate School, HIT. From 2016 to 2017, he was with the School of Electrical and Information Engineering, University of Sydney, Sydney, Australia, as a China Scholarship Council Visiting Scholar. Since 2017, he has been an Assistant Professor with the Department of Electrical and Information Engineering, Shenzhen Graduate School, HIT. His current interests include error control codes, space information networks, random multiple access, and machine-to-machine communications. He received the Shenzhen High Level Talent Program Award in 2015.

ZIXUAN HUANG received the bachelor's degree in electronic information science and technology from the Hefei University of Technology, Hefei, in 2016. She is currently pursuing the master's degree with the Communication Engineering Research Centre, School of Electrical and Information Engineering, Harbin Institute of Technology, Shenzhen, China. Her research interests include space information networks, error control codes, and machine-to-machine communications.

SHAOHUA WU (S'07–M'11) received the Ph.D. degree in communication engineering from the Harbin Institute of Technology in 2009. From 2009 to 2011, he held a post-doctoral position at the Department of Electronics and Information Engineering, Shenzhen Graduate School, Harbin Institute of Technology, where he has been an Associate Professor since 2012. His current research interests include wireless image/video transmission, deep space communication, IR-UWB ranging/localization/communication, and 5G wireless transmission technologies.

QINYU ZHANG (M'08–SM'12) received the bachelor's degree in communication engineering from the Harbin Institute of Technology (HIT) in 1994 and the Ph.D. degree in biomedical and electrical engineering from the University of Tokushima, Japan, in 2003. From 1999 to 2003, he was an Assistant Professor with the University of Tokushima. From 2003 to 2005, he was an Associate Professor with the Shenzhen Graduate School, HIT, and the Founding Director of the Communication Engineering Research Center, School of Electronic and Information Engineering. Since 2005, he has been a Full Professor, and serves as the Dean for the EIE School. His research interests include aerospace communications and networks, wireless communications and networks, cognitive radios, signal processing, and biomedical engineering. He has been a TPC Member of INFOCOM, ICC, GLOBECOM, WCNC, and other flagship conferences in communications. He has received the National Science Fund for Distinguished Young Scholars, the Young and Middle-Aged Leading Scientist of China, the Chinese New Century Excellent Talents in University, and three scientific and technological awards from governments. He was a TPC Co-Chair of the IEEE/CIC ICCC'15, a Symposium Co-Chair of the IEEE VTC'16 Spring, an Associate Chair of the Finance of ICMMT'12, a Symposium Co-Chair of CHINACOM'11, and a Founding Chair of the IEEE Communications Society Shenzhen Chapter. He is on the Editorial Board of some academic journals, such as the *Journal on Communications*, the *KSII Transactions on Internet and Information Systems*, and *Science China Information Sciences*.